Journal of Catalysis **194,** 452–460 (2000)
doi:10.1006/jcat.2000.2930, available online at http://www.idealibrary.com on IDEAL®

In Situ Investigations of Structural Changes in Cu/ZnO Catalysts

J.-D. Grunwaldt,[1] A. M. Molenbroek, N.-Y. Topsøe, H. Topsøe, and B. S. Clausen

Haldor Topsøe Research Laboratories, Nymøllevej 55, DK-2800 Lyngby, Denmark

Received March 23, 2000; revised May 17, 2000; accepted May 17, 2000

Dynamic changes in the structure and catalytic activity of Cu/ZnO methanol synthesis catalysts have been investigated by a further developed *in situ* method, which combines X-ray diffraction (XRD), X-ray absorption fine structure spectroscopy (XAFS), and on-line catalytic measurements by mass spectrometry. The temperature-programmed reduction of copper was monitored both by *in situ* quick-EXAFS (QEXAFS) and on-line mass spectrometry. The results indicate that under typical mild reduction conditions very small copper particles (10–15 Å) are formed. Upon change in the reduction potential of the methanol synthesis gas, reversible changes of the Cu–Cu coordination number are observed by EXAFS. These structural changes are accompanied by changes in the catalytic activity and the highest activities were observed after exposure to the most reducing conditions. In this state the catalyst exhibited low Cu–Cu coordination numbers. These results support the model that reversible changes in the wetting of ZnO by Cu may occur upon changes in the reaction conditions. The results also show that such dynamical changes in Cu morphology may influence the catalytic properties. All the conditions used in the above studies are less severe than those observed to result in bulk alloy formation. However, additional XAFS measurements at higher temperatures have been performed and EXAFS spectra have been simulated to address the possibility for Cu–Zn alloy formation as suggested by recent results in literature. Only under severe reduction conditions was significant alloying of copper and zinc observed in EXAFS in addition to the morphological changes. Such changes have not been seen in the Cu/SiO_2 system.

1. INTRODUCTION

Copper-based methanol synthesis catalysts have been subject to numerous investigations (see, e.g., Refs. (1–23)). Especially for the important Cu/ZnO-based catalysts different copper species have been proposed concerning the active center during the methanol synthesis reaction, such as a Cu^+ species dissolved in ZnO (1, 10), a Cu^- species at the so-called Schottky junction (7) between copper and the semiconducting oxide support, or Cu^0 supported on the ZnO phase (2, 4–6, 8, 9, 16–18). Recently, it has been considered that Cu may also be alloyed with Zn, possibly only at Cu surfaces (13, 14, 19, 20). Also, ZnO on top of Cu^0 has been suggested (22, 23).

In situ X-ray absorption fine structure results have directly shown that Cu particles supported on ZnO and on SiO_2 are in the metallic state (5, 8, 24). Nørskov and coworkers (17, 25) formulated a microkinetic model for the methanol synthesis reaction, using surface science data on Cu single-crystal surfaces. They showed that the model could account for most of the results on different Cu-based catalysts, also from laboratory pilot plants. However, in the case of ZnO-containing catalysts, measured and calculated results were different (11). Under more reducing conditions the model predicted too low methanol formation rates and under oxidizing conditions they were too high.

Previous extended X-ray absorption fine structure (EXAFS) results have shown that Cu particles supported on SiO_2 and ZnO respond differently to changes in the reduction potential of the synthesis gas (24). Whereas the particles on SiO_2 did not show significant change in particle morphology as a function of the reduction potential of the reaction mixture, Cu particles supported on ZnO significantly change their structure. The morphological changes could be explained by a simple model, based on changes in the relative surface and interface energies (24). The dynamic behaviour of the Cu/ZnO system has recently also been reported in other studies (13, 20, 23, 26, 27).

Incorporating such dynamic changes, a dynamic microkinetic model based on the surface science measurements could be developed (11), which provided a much better description of the measured rates of methanol formation. The dynamic model considers the changes in surface area and the higher activity of Cu(110) and Cu(100), compared to Cu(111) planes (18, 28). Under reducing conditions the formation of oxygen vacancies at the Cu–ZnO interface probably results in an increased interaction with the copper particles and the formation of more disk-like particles with higher surface areas. Cu–Zn alloying may also play a role since Nakamura *et al.* (19) reported in a surface science study that the activity of Zn deposited on Cu(111) was higher than that of a clean Cu(111) surface. They recently also reported data that suggest higher reaction rates on Cu–Zn alloy catalysts, structurally analysed by XRD (14). Recent FTIR studies also show the formation of a

[1] To whom correspondence should be addressed. Fax: +45-45 27 29 99. E-mail: jdg@topsoe.dk.

0021-9517/00 $35.00

Cu–Zn surface alloy under severe reduction conditions and it was found that the formation/destruction of the surface alloy may be reversible (13, 20).

To understand the catalytic properties of Cu/ZnO-based catalysts in more detail and to facilitate the establishment of links between the structural and catalytic properties, we have continued the *in situ* characterization studies and expanded them with on-line activity measurements. Both XRD and XAFS techniques give the possibility to perform the studies *in situ* under actual reaction conditions (29–33). In such studies the choice of the *in situ* cell is crucial (29, 34). Since small capillary microreactors offer ideal conditions for catalysis (plug flow, rapid temperature change, small temperature and concentration gradients, etc.) and ensure that the structural information is obtained on exactly the same part of the sample responsible for the catalysis, realistic catalytic and structural information can be obtained simultaneously on the same samples (29, 35). Since XRD probes structures with long-range order and EXAFS is sensitive mainly to the local surroundings of the atoms in the material, they are complementary techniques and the combined use of the two techniques provides a more complete structural description of the catalyst (34). Furthermore, to follow dynamical effects, it is advantageous to replace the normal EXAFS technique with the QEXAFS technique (36). The combined XRD–QEXAFS technique was first decribed in (30).

In the present study we have used the above-mentioned plug flow microreactor and combined the XRD/(Q)EXAFS techniques simultaneously with on-line product analysis using mass spectrometry. The combined use of the techniques will first be illustrated by studies of the temperature-programmed reduction (activation) of the copper catalysts. Subsequently, the structural and catalytic properties of the activated samples are investigated under synthesis conditions with gas compositions adjusted to provide different reduction potentials. The question of Cu/Zn alloy formation is explored by reduction experiments at higher temperatures. A comparison with simulated XAFS spectra using the FEFF package (37) and with previous FTIR results (13, 20) is also performed.

2. EXPERIMENTAL

The combined XAFS/XRD experiments with on-line catalytic measurements were performed at HASYLAB, DESY (Hamburg, Germany) using synchrotron radiation at beamline X1 from the DORIS III storage ring.

Figure 1 depicts a schematic drawing of the setup for the combined (Q)EXAFS/XRD studies with on-line product analysis. Since it is an extension of previously shown setups (29, 30), only the general setup will be discussed. The central part is the quartz capillary containing the catalyst sample, which serves both as the microreactor and as the cell for

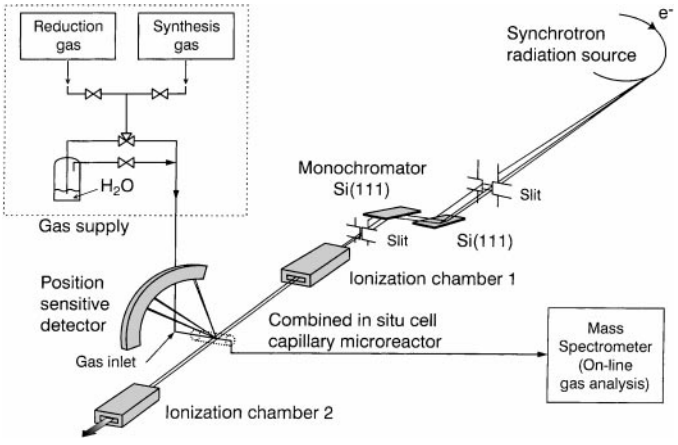

FIG. 1. Schematic setup of the experimental setup for combined *in situ* QEXAFS/XRD studies with on-line mass spectrometric analysis (partly adapted from Clausen *et al.* (30)).

the *in situ* XAFS/XRD measurements. The setup allows on-line catalytic measurements during both transient and steady state operation.

The reaction cell consisted of a quartz capillary tube (typical diameter, $\phi = 0.5$ mm; wall thickness, $t = 0.02$ mm), in which the catalyst (2–4 mg, sieved fraction, 75–125 μm) was loaded and kept in place by two plugs of glass wool. From the gas preparation system different premixed gases could be led through the capillary reactor cell. Typically, a flow of 5 ml/min was used. Product analysis was performed by mass spectrometric analysis (Balzers Thermostar). Heating of the combined *in situ* cell/microreactor to 600°C was performed by passing preheated N_2 gas over the capillary shielded with a graphite hood.

The XAFS data were obtained in transmission geometry, and the XRD pattern was obtained by a position-sensitive detector (INEL CPS120) above the sample (Fig. 1). The X-rays were monochromatized by two Si(111) crystals. The content of higher harmonics in the monochromatized beam was diminished by slightly detuning the two crystals from the parallel position.

For XAFS measurements at the Cu, K edge (8.9803 keV) the incident and transmitted X-rays were recorded by use of N_2-filled ionization chambers. An Yb_2O_3 reference sample, inserted between the second and third ionization chamber, was used for energy calibration. XAFS spectra were recorded between 8700 and 9660 eV by step scanning the monochromator. While conventional XAFS was used when the sample was at constant temperature, quick-EXAFS data (35, 36) were collected *in situ* during reaction (reduction) and heating of the sample in the region 8700–9600 eV by moving the monochromator at a constant angular speed.

Fourier transformation was applied on the k^1 weighted $\chi(k)$ function in the interval $k = 2.5$–12.0 Å^{-1}. The peak in the Fourier-transformed data was filtered (interval

1.0–3.0 Å) and then inversely Fourier-transformed back into the *k* space. The backscattering amplitudes and phase shifts of the Cu–Cu and Cu–Zn wavefunctions were taken from a Cu foil as a reference (coordination number 12; Cu–Cu distance, 2.55 Å). The amplitude function and backscattering amplitude for Zn are very similar (38) since Cu and Zn metals are neighbours in the periodic table. Additionally, EXAFS spectra were recorded on a $Cu_{63}Zn_{37}$ bulk alloy.

In situ XRD spectra were collected between two successive EXAFS or QEXAFS scans by fixing the energy at 8.7 keV ($\lambda = 1.425(07)$ Å). The energy was chosen below the Cu,K edge to prevent fluorescence from the copper in the sample. A position-sensitive detector (INEL CPS120) with an angular distance between the channels of 0.03° was used to collect the XRD spectra over a *d*-range of 5.45 Å–0.77 Å. For later data analysis we used the 2θ range 15–105°.

Throughout this study a Cu/ZnO catalyst with 4.5 wt% Cu loading was used, prepared by coprecipitation of an aqueous solution of Cu– and Zn–nitrates according to a procedure given in Ref. (39) and calcined for 1 h at 300°C. The Cu/SiO_2 catalyst (∼5 wt% Cu), used for comparison, was prepared according to a procedure given by Geus and co-workers (40).

The catalyst was reduced in 0.5% CO, 5% CO_2, and 4% H_2 in Ar at ambient pressure. After rapid heating to 120°C (2°C/min; holding time, 10 min), the catalyst was further reduced with a heat ramp of 0.5°C/min to 220°C (holding time, ca. 1 h). After reduction, the catalyst was cooled to room temperature and the gas was switched to a methanol synthesis gas containing either 5% CO and 5% CO_2 in hydrogen ("dry" syngas) or a mixture containing 3% H_2O, 4.85% CO, and 4.85% CO_2 in hydrogen ("wet" synthesis gas). The methanol synthesis reaction was carried out at 220°C after the mixture was heated from room temperature to 220°C (ramp, 5°C/min). Furthermore, in separate experiments the Cu/ZnO and the Cu/SiO_2 sample were heated up to 600°C in 10%CO/90%H_2 (ramp, 5°C/min) to study possible alloy formation.

3. RESULTS AND DISCUSSION

3.1. *Reduction of the Copper Catalyst as Studied by TPR/QEXAFS/XRD*

Figures 2–4 show the TPR of the Cu/ZnO catalyst, as monitored by on-line mass spectrometry (Fig. 2), a selection of Fourier-transforms of the simultaneously recorded QEXAFS spectra above the Cu,K edge (Fig. 3), and a selected *in situ* XRD diffractogram (Fig. 4). The traces of water ($m/e = 18$) and hydrogen ($m/e = 2$) show that the reduction of the catalyst starts around 180°C, which is substantiated by changes in the EXAFS spectra. The peak at $R = 1.7$ Å in Figs. 3a–3d, attributed to the Cu–O shell, disappears at 220°C. Simultaneously, a new peak at $R = 2.2$ Å

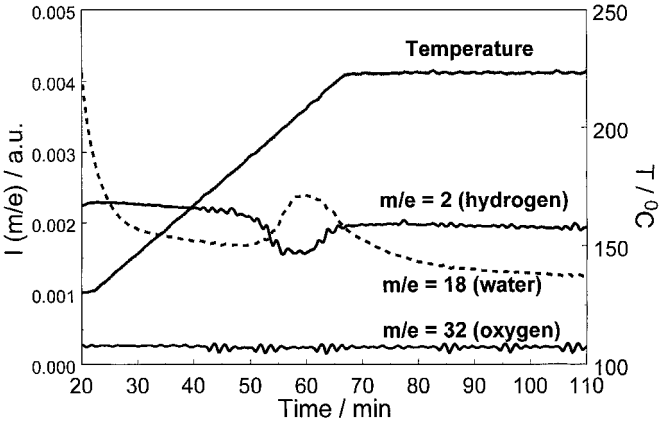

FIG. 2. Temperature-programmed reduction of a CuO/ZnO precursor catalyst in a reduction gas (0.5% CO, 5% CO_2, 4% H_2 in Ar, 0.5°C/min), shown are traces of hydrogen ($m/e = 2$), water ($m/e = 18$), and oxygen ($m/e = 32$), and the corresponding temperature; on-line analysis was performed simultaneously to analysis with QEXAFS (Fig. 3) and XRD (Fig. 4).

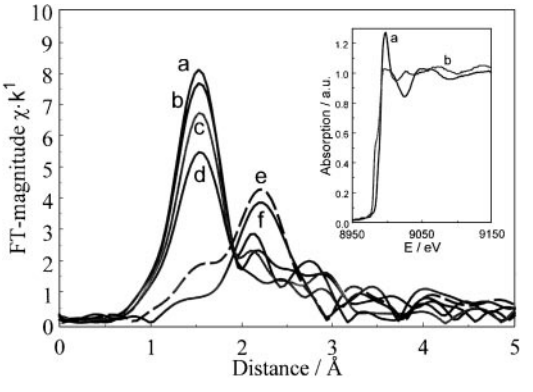

FIG. 3. Magnitude of the Fourier-transformed data (k^1 weighted) of selected *in situ* QEXAFS spectra at the Cu,K edge of a Cu/ZnO catalyst during reduction in 0.5% CO, 5% CO_2, 4% H_2 in Ar: a, 120°C; b, 130°C; c, 180°C; d, 195°C; e, 210°C; f, 220°C; the inset shows the QEXAFS spectra before (a, 120°C) and after (b, 220°C) reduction.

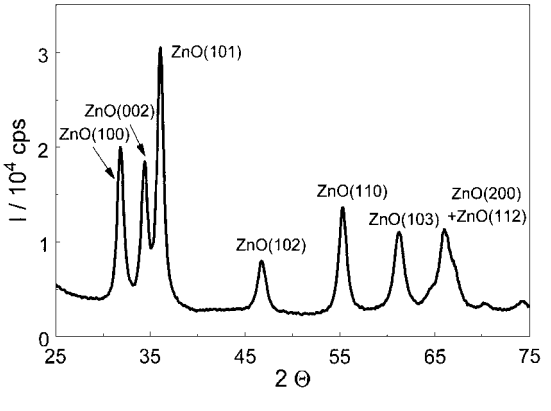

FIG. 4. *In situ* XRD pattern of the copper catalyst after TPR at 220°C.

appears, representing the first Cu–Cu shell (Figs. 3e and 3f). Note that the distance scale in the Fourier-transformed spectra was not corrected for the phase shift. The peak at $R = 1.7$ Å is reported in Ref. (3) and is very typical for Cu–O in CuO or Cu-doped ZnO, which is probably formed during the previous calcinations of the catalyst. The reduction of the Cu(II) phase is also reflected by the raw QEXAFS spectra, where the strong white line due to Cu(II) disappears and the edge is shifted to lower energies from 8986 to 8980 eV due to Cu metal formation (shown as inset in Fig. 3). Also, the stronger oscillations due to the Cu metal are visible in the inset. Hence, both on-line mass spectrometry and EXAFS data show the formation of metallic Cu particles at about 200°C. Furthermore, the reduction temperature is quite high, showing that the reduction potential of the gas is low. Using pure hydrogen, this peak would be shifted to ~140°C.

In XRD only the ZnO phase is observable after reduction at 220°C (Fig. 4). The lack of diffraction lines of copper metal (and copper oxide before reduction) is in view of the EXAFS results due to the presence of very small particles. The use of a gas with a higher reduction potential (e.g., 10% CO/90% H_2) or a higher heating ramp led to a clear Cu(111) line around $2\Theta = 43°$ and therefore larger Cu crystallites (cf. also (29)). The volume-averaged crystallite size of the ZnO phase was found to be about 80 Å, as calculated from the half-width of the (110) diffraction line by the Debye–Scherrer formula (41).

The reduction of copper in Cu/ZnO catalysts is well documented in the literature (e.g., (24)), but is shown here as an illustrative example of the simultaneous use of QEXAFS/XRD and on-line product analysis on the *same* sample. The reduction of copper occurs over a ca. 30°C narrow temperature range and can be followed both by *in situ* EXAFS and TPR. Furthermore, EXAFS and XRD give information on the phase identity and the particle/crystallite size of the phases present in the Cu/ZnO system.

Further analysis of conventional EXAFS data on the Cu/ZnO catalyst after reduction at 220°C reveals by fitting with amplitude and phase functions extracted from a copper foil that the apparent Cu–Cu coordination number is around 6 and the Cu–Cu distance is 2.54 Å (Table 1). The particle size can be estimated from the coordination number of copper by calculating of the coordination numbers of different spherically truncated copper clusters and by considering that the atomic motion in small particles is anharmonic (30, 42, 43). Clausen and Nørskov (43) recently developed a model to calculate the true coordination number for a fcc metal from the apparent coordination number by using a linear proportionality factor and the linear expansion coefficient α. In the present case, this results in a "true" coordination number of about 8.5, corresponding to a particle size of 10–15 Å. The absence of diffraction lines from Cu phases in the XRD, which are observed when the catalyst is treated under more severe conditions or at a higher ramp rate, indirectly confirms the presence of small copper crystallites (<20–30 Å). The small copper particles also easily re-oxidize at room temperature in traces of oxygen, which is another indication of the small particle size (cf. (44)). These results also illustrate the necessity to obtain structural information under *in situ* conditions.

TABLE 1

Apparent Coordination Numbers ($N_{Cu–Cu}$), Cu–Cu Distance ($R_{Cu–Cu}$), Vibrational Amplitude ($\Delta\sigma_1$), and Energy Shift, ΔE_1, Obtained by Fitting the First Cu–Cu Shell of the EXAFS Data of the Cu/ZnO Catalyst after Different Treatments

Treatment	$N_{Cu–Cu}$ (±0.5)	$R_{Cu–Cu}$ (Å) (±0.02)	$\Delta\sigma_1$ (Å) (±0.01)	ΔE_1 (eV)
Reduction gas	6.1	2.54	0.10	0.47
1st dry syngas	5.3	2.53	0.09	1.38
1st wet syngas	8.3	2.55	0.10	−0.10
2nd dry syngas	6.9	2.58	0.09	−1.75
2nd wet syngas	8.8	2.55	0.09	0.32
3rd dry syngas	6.3	2.57	0.09	−2.17
3rd wet syngas	7.7	2.57	0.09	−1.17

To sum up, these studies demonstrate that *in situ* XRD/QEXAFS and on-line product analysis measurements can be used to give valuable chemical and structural information during TPR. Also, the present reduction procedure is seen to result in very small metallic copper particles on ZnO, ideal for the studies reported below.

3.2. Reversible Change in Morphology in Dry and Wet Synthesis Gas

Upon a change from reduction gas (0.5% CO, 5% CO_2, and 4% H_2 in Ar) to synthesis gas (5% CO, 5% CO_2, balance H_2) at room temperature, the catalyst starts to produce methanol (and water) at 220°C as monitored by the traces $m/e = 31$ and 18 with on-line mass spectrometry (Fig. 5a). The EXAFS spectra (curves a and b in Fig. 6) and powder X-ray diffraction patterns (curves a and b in Fig. 7) reveal that the average particle size remains small upon a change in the gas composition because the apparent coordination number of the nearest Cu–Cu neighbours stays small (Table 1) and no Cu diffraction lines appear in the XRD pattern.

To study possible reversible changes in the structure and activity as functions of the reduction potential of the gas, the gas mixture was varied in the next steps by using either "dry" or "wet" syngas conditions. The gas composition was changed at room temperature, respectively. The response in the mass spectrum is shown in Figs. 5b–5d. The relative scale for the MS intensities has been held constant. Upon exposure of the catalyst to wet syngas, the catalytic activity significantly decreased (Fig. 5b). The trace of methanol increased significantly again when the catalyst was once more

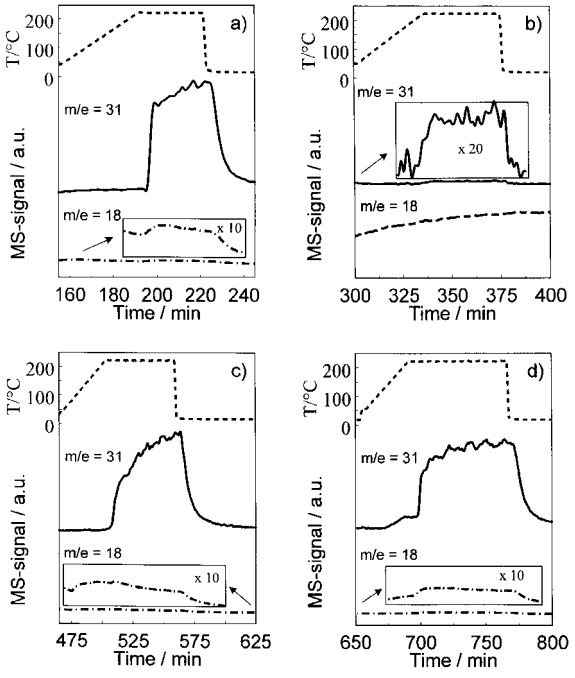

FIG. 5. On-line catalytic analysis of the product stream on a Cu/ZnO catalyst: (a) change to "dry" synthesis gas (1st cycle); (b) change to "wet" synthesis gas (1st cycle); (c) change to "dry" synthesis gas (2nd cycle); (d) repeated heating in "dry" synthesis gas (shown are the heating ramp and the traces of methanol and water; the scale for the MS intensity has been held constant in all figures; insets show magnified curves).

tested under dry syngas (Fig. 5c). This reversible behaviour under dry and wet syngas conditions could be repeated in further steps. Note that there is a slow transient state in the mass spectrometer signal of methanol when one is changing from wet to dry syngas (Fig. 5c). This is not due to the prior temperature change since it was not observed when the same temperature change was performed in dry syngas (Fig. 5d). The water signal increases before the signal

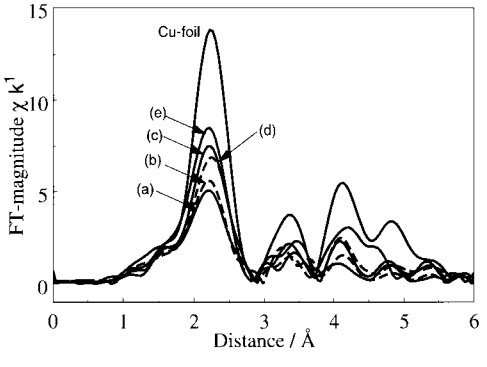

FIG. 6. Fourier transformed $\chi(k) \cdot k$ of the *in situ* EXAFS data at the Cu,K-edge of the Cu/ZnO catalysts, recorded simultaneously to on-line gas analysis: (a) in reduction gas; (b) after change to "dry" synthesis gas (1st cycle); (c) after change to "wet" synthesis gas (1st cycle); (d) after change to "dry" synthesis gas (2nd cycle); (e) after change to "wet" synthesis gas (2nd cycle).

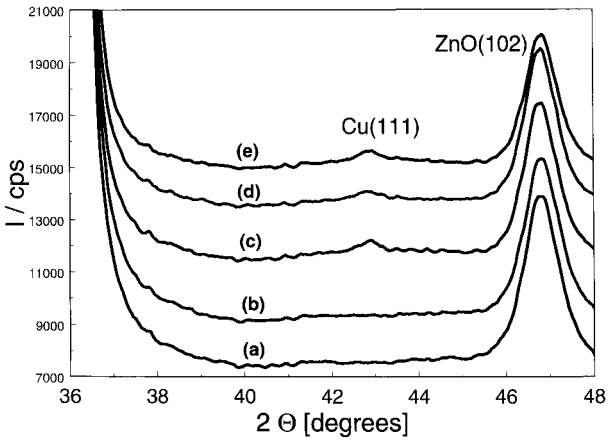

FIG. 7. *In situ* XRD data, recorded parallel to on-line analysis and EXAFS: (a) in reduction gas; (b) after change to "dry" synthesis gas (1st cycle); (c) after change to "wet" synthesis gas (1st cycle); (d) after change to "dry" synthesis gas (2nd cycle); (e) after change to "wet" synthesis gas (3rd cycle).

for methanol does (Fig. 5c), probably due to desorption of some water. The trace of water is, however, significantly lower than that in Fig. 5b.

Simultaneous to the catalytic studies, EXAFS and XRD studies were performed. The Fourier-transformed EXAFS spectra in Fig. 6 reveal in perfect agreement with previous studies (24) that reversible structural changes occurred when the reduction potential of the synthesis gas was changed. When one changed from dry syngas to wet syngas, the apparent coordination number in EXAFS increased (Fig. 6c, Table 1). Also, in XRD a weak diffraction line due to a metallic Cu phase was observed upon this change (Fig. 7c). The increase in the apparent coordination number of Cu is to a large extent reversible when changing back to dry syngas (Fig. 6d). Due to the very broad XRD diffraction lines, it is more difficult to observe significant changes by XRD than by EXAFS. The ZnO phase did not show any detectable changes in XRD when exposed to the different gaseous conditions.

Figure 8 gives an overview of the change in the apparent Cu–Cu coordination number of the nearest neighbours in EXAFS together with the simultaneous change in catalytic activity. These results clearly show reversible changes both in the activity and in the structure of the Cu particles. Besides the reversible changes, it is observed that the coordination number tends to increase with the number of cycles (Table 1, Fig. 8), and this is accompanied by a decrease in the overall activity of the catalyst (Fig. 8). This indicates sintering of the copper particles (24), which probably occurs more rapidly when water is added to the feed. This is also supported by the XRD data.

The results show that the reversible structural changes are linked to changes in the gas composition. Under more reducing conditions the apparent coordination number is

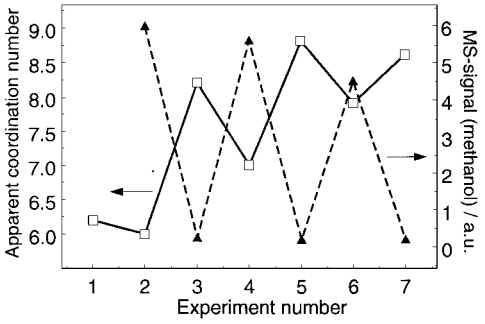

FIG. 8. Change of apparent coordination number of the Cu–Cu shell (extracted from EXAFS analysis) and the relative methanol formation dependent on the gas conditions: (1) reduction gas; (2), (4), and (6), dry synthesis gas; (3), (5), and (7), wet synthesis gas.

lower, whereas under more oxidizing conditions the apparent coordination number is higher. These observations are in line with the wetting/nonwetting of Cu particles on the ZnO support (24), which can schematically be seen in Fig. 9 (sketches a and b). Figures 9a and 9b show that an increase of the oxidation potential (wet syngas) leads to more spherically shaped particles with higher apparent Cu coordination number. When the water partial pressure is lowered, the more reducing conditions lead to the formation of more

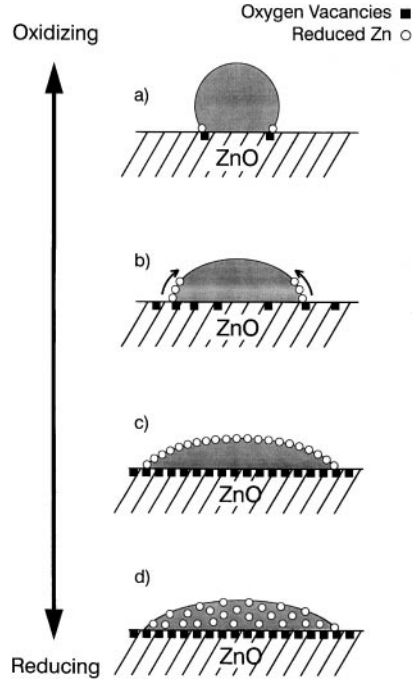

FIG. 9. Schematic model for the wetting/nonwetting of the Cu particles on the Zn support, surface alloying, and bulk alloy formation: (a) round-shaped particle under oxidizing syngas conditions; (b) disk-like particle under more reducing conditions; (c) surface Zn–Cu alloying due to stronger reducing conditions; (d) brass alloy formation due to severe reducing conditions.

disk-like particles. These have a relatively higher concentration of surface atoms with low coordination numbers and this gives rise to a lower apparent coordination number in EXAFS. A simple explanation can be drawn from the calculation of the relative surface and interface energies of a Cu particle on ZnO (11, 24). The shape of the Cu particles can be found by the Wulff construction (45), when the changes in the contact surface free energy are considered. The results are given in Ref. (11) and it has been shown that the change in contact surface energy is related to the changes in the number of oxygen vacancies at the interface as a result of changes in the gaseous conditions (11, 24). The formation of oxygen vacancies under these conditions is supported by previous IR transmission results because the IR transmittance drops significantly under more reducing conditions (20, 46) and also shows reversible changes (20). The simultaneously recorded XRD patterns did not provide unambiguous support for this explanation due to the small Cu particle size but showed clearly that sintering occurred during the oxidation/reduction cycles. Flat Cu particles under reduction conditions have also been reported by Yurieva *et al.* (27, 47).

As Fig. 8 clearly shows, lower activities were observed after exposure to the most oxidizing conditions ("wet" syngas). Since water does not absorb strongly on Cu (11, 12), this observation is not likely to be due to a simple inhibition by water. Hence, it is suggested that the differences in catalytic activity are not only due to changes of the gas mixture but may also be related to changes in the morphology observed by EXAFS and explained by the wetting/nonwetting of the copper particles on the ZnO support (Fig. 9). Under most reducing conditions, the flat particles result in a higher copper surface area and, as concluded from the Wulff construction (11, 24), a higher degree of the more active Cu(100) and Cu(110) planes. Also, the comparison of measured rates on Cu/ZnO-based catalysts and those calculated from a microkinetic model has shown that the rate of methanol formation cannot be explained by considering stationary copper particles, but the results could be explained when the wetting/nonwetting and the structure sensitivity are taken into account (11). This dynamic model could also explain observations for industrial $Cu/ZnO/Al_2O_3$ catalysts, where it was noticed that in the most reducing synthesis gas mixtures the measured rates were larger than those predicted by a static microkinetic model (11). Also, the transient behaviour after a change from more reducing to less reducing synthesis gas supports this hypothesis (12). In this case a peak of higher methanol activity is found when a change is made from the more reducing gas (5% CO, 95% H_2) to the less reducing methanol synthesis gas conditions (5% CO, 5% CO_2 in H_2). Finally, it could be added that the transient state observed during the on-line catalytic measurements in the present study also indicates that morphology changes of the catalyst take place

(compare Figs. 5b and 5c). The rate of methanol formation increases slowly when the gas is switched from wet to dry synthesis gas. After several reduction/oxidation cycles, this transition takes longer, probably because the particles are larger and restructuring is slower. Hence, the differences in catalytic activity seem to be not only due to change of the gas mixture but also due to morphology changes.

3.3. *Possibilities of Alloying in the Cu/ZnO System*

Recent FTIR studies on similar samples (13, 20) suggest that in addition to the above-described wetting/nonwetting phenomena reversible formation and destruction of surface (and possibly bulk) alloying may play a role in the Cu/ZnO system under more severe reducing conditions. This is also illustrated in Fig. 9. The presence of Cu–Zn alloys was also recently suggested by Nakamura and co-workers (14, 19). Analysis of the *in situ* EXAFS results (Table 1), recorded under different reaction conditions, shows that the large changes in coordination numbers are not accompanied by large changes in the Cu–Cu distances. In fact, in all cases the Cu–Cu bond length is quite constant (2.56 ± 0.03 Å) and agrees well with the Cu–Cu bond length in metallic copper ($R_{\mathrm{Cu-Cu}} = 2.55$ Å). Since the Zn–Cu distance in the Cu–Zn alloy is expected to be 0.1 Å longer than the Cu–Cu distance (48, 49), the present EXAFS results indicate that no significant bulk alloying is present under any of the conditions used in the experiments discussed above. To elucidate further the sensitivity of the EXAFS spectra to possible alloying in the Cu/ZnO system, we will discuss below simulated Cu–Zn EXAFS spectra as well as experimental studies of a CuZn alloy. Cu/ZnO and Cu/SiO_2 catalysts have additionally been investigated after reduction treatment up to 600°C.

EXAFS spectra of Cu and Cu–Zn alloys were simulated using the FEFF 6 package (37). Figure 10 shows the results. In the first part (Fig. 10-1), the effect of different nearest neighbours is considered examining different clusters. In Fig. 10-2 bulk samples with different neighbour shells are examined. In the spectra of Fig. 10-1 the EXAFS spectra of different $Cu(Cu_{1-x}Zn_x)_{12}$ clusters were calculated in the following way to estimate the influence of Zn-neighbouring atoms. The central atom of interest is Cu and only the first shell in the fcc lattice is considered. Hence, the Cu atom is surrounded by 12 neighbouring atoms. Molecular dynamics simulations of small Cu particles in previous studies (50) have only predicted small changes in the average bond lengths and therefore we assume for the simulations performed in this section that the Cu–Cu and Cu–Zn distances are similar to that determined in bulk metals/alloys.

When curve a in Fig. 10-1 is compared to curve a in 10-2, it appears that the first shell represents the contributions around 2.2 Å and that multiple scattering effects are of minor importance. Curve c in Fig. 10-1 shows the simulation of the spectra when the central Cu atom is surrounded by

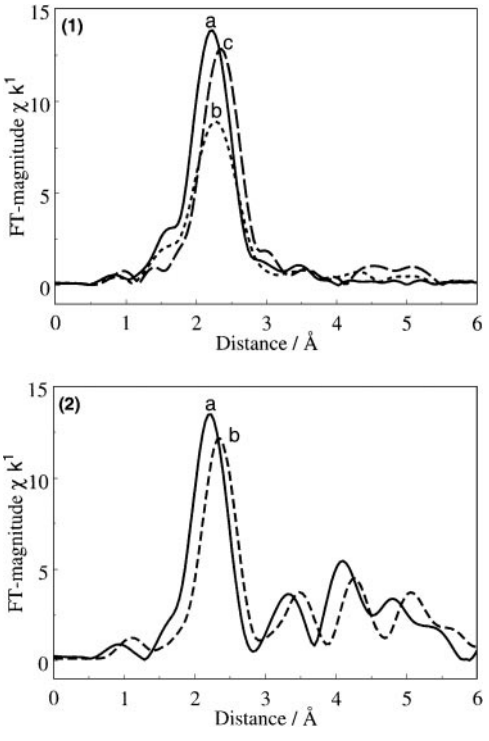

FIG. 10. Simulated Fourier-transformed XAFS spectra of Cu and Cu–Zn for elucidating the effects for alloying: (1a) $Cu(Cu)_{12}$ cluster; (1b) Cu (Cu_6Zn_6) cluster; (1c) $Cu(Zn)_{12}$ cluster; (2a) Cu bulk; (2b) Cu–Zn alternating shells (see text).

12 Zn atoms (here called "$Cu(Zn)_{12}$ cluster") with a distance $R_{\mathrm{Cu-Zn}} = 2.66$ Å (as calculated from the atomic radii of Cu and Zn (48)). Since Cu and Zn are neighbours in the periodic table, amplitude functions and backscattering amplitudes are very similar (38). Only the interatomic distance is slightly different, resulting in a small shift to higher R values. A $Cu(Zn)_{12}$ with the hypothetical distance $R = 2.55$ Å (distance between two copper atoms in bulk metal) gives therefore a similar FT EXAFS spectrum as a $Cu(Cu)_{12}$ cluster. Taking a $Cu(Zn_6Cu_6)$ cluster with 6 Cu atoms in the first shell ($R_{\mathrm{Cu-Cu}} = 2.55$ Å) and 6 Zn in the first shell ($R_{\mathrm{Cu-Zn}} = 2.66$ Å), again a shift to higher R values is discerned (curve b in Fig. 10-1); however, some changes in intensity are observed due to the different distances used in the model. These calculations show that alloying can be observed by a shift of the peaks in the Fourier-transformed EXAFS spectra.

Comparing the Fourier-transformed EXAFS spectra of Cu/SiO_2 (Fig. 11a) and Cu/ZnO (Fig. 11b) after the catalyst is heated in 10% CO/H_2 to 600°C, a clear shift is found in the peaks in the case of Cu/ZnO. The Cu/ZnO catalyst clearly forms an alloy, as concluded from the shift and also by comparison with the data of the $Cu_{68}Zn_{32}$ alloy (Fig. 11c), whereas the Cu/SiO_2 catalyst only contains metallic copper. The fit of the Fourier-backtransformed spectrum of Cu/ZnO results in a Cu–Zn distance of $R = 2.64$ Å.

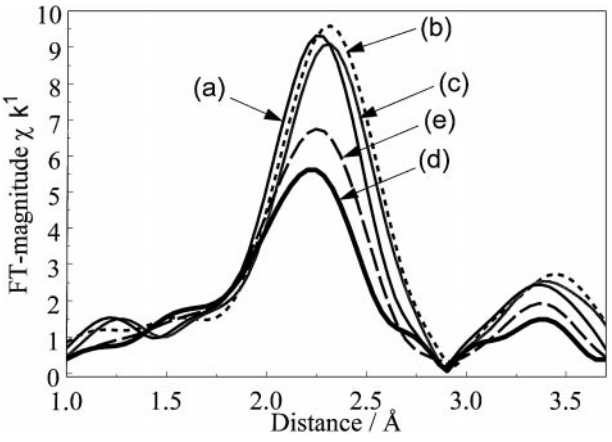

FIG. 11. Fourier transform of the EXAFS spectra at the Cu edge of (a) Cu/SiO_2, (b) Cu/ZnO, (c) $Cu_{68}Zn_{32}$, (d) Cu/ZnO (dry synthesis gas conditions at 220°C, 1st cycle), and (e) Cu/ZnO (after reduction in reduction gas at 300°C); (a) and (b) were heated to 600°C in 10% CO/H_2.

Comparing the spectra of the Cu/ZnO catalysts treated at 220°C in dry and in wet syngas, shows however no measurable shift. As an example, the Fourier-transformed EXAFS spectrum of the Cu/ZnO catalyst, treated at 220°C in synthesis gas, is shown in curve d in Fig. 11. The fit of the Cu–Cu shell shows furthermore that the Cu–Cu distance is quite similar to that of metallic bulk copper ($R = 2.55$ Å, Table 1) and not to that of an CuZn alloy ($R = 2.66$ Å). Therefore, we can exclude significant Cu–Zn bulk alloying of the Cu/ZnO catalyst at typical reaction temperatures.

In the next step we investigated by EXAFS the Cu/ZnO catalyst after treatment in the reduction gas at temperatures between 220 and 400°C and compared the results to previous FTIR studies (20) of CO adsorption on similar catalysts and under similar reaction conditions. In EXAFS only an increase in coordination number and therefore a larger Cu particle size was observed when the reduction temperature was increased. The Fourier-transformed EXAFS spectrum after treatment at 300°C is shown in curve e of Fig. 11. No shift of the peak of the first shell in the Fourier-transformed EXAFS spectra to higher R values was found. This again excludes the formation of a bulk alloy with significant amounts of Zn by EXAFS.

After reduction of the Cu/ZnO catalyst at 220°C, a CO absorption band at about 2096 cm^{-1} with a lower frequency shoulder is observed by FTIR (20). The band at 2096 cm^{-1} is typical for linearly adsorbed CO on Cu^0 sites on Cu(110) planes (20, 51). When the reduction temperature was increased to 300°C, significant downward frequency shifts and a decrease in intensity in the CO bands were observed. It was argued (13, 20) that this result cannot be solely explained by changes in the relative distribution of the Cu surface planes. Instead, a more likely explanation is the migration of zinc onto the surface of the Cu particles, resulting in the formation of a Cu–Zn surface alloy (13).

Thus, with increasing reduction temperature, Zn seems to migrate onto the copper particles, forming at about 300°C a surface alloy as evidenced by FTIR and at higher temperatures a bulk alloy as shown by EXAFS. This possible surface brass formation has also been reported in surface science studies (14, 19, 52) and is supported by preliminary DFT calculations (20). Also, Viitanen *et al.* (22) have recently shown in a low-energy ion-scattering (LEIS) study that the copper particles are more enriched by Zn when the reduction temperature is increased. They interpret that Zn is present as ZnO (22, 23). In fact, Cu–Zn surface alloys are able to absorb oxygen (21). Poels and co-workers (22, 23) have recently also reported that a catalyst reduced at 427°C compared to 327°C exhibited higher activity in methanol synthesis. This effect is even higher in the case of ester hydrogenolysis (23). Hence, both wetting/nonwetting phenomena and surface alloying seem to play a crucial role in the Cu/ZnO system at reaction temperatures higher than those typically used in methanol synthesis.

4. CONCLUSIONS

Using a capillary microreactor serving as an *in situ* cell, both structural (Q)EXAFS/XRD analysis and on-line catalytic measurements by mass spectrometric analysis have become possible. Studies can be performed on the *same* sample under *identical* conditions, as illustrated by the temperature-programmed reduction and catalysis studies of the Cu/ZnO catalysts. The combination of the complementary XRD and EXAFS/QEXAFS techniques allows a more complete structural description of the catalyst and the combination with on-line catalytic measurements allows the establishment of structure–activity relationships.

Specifically, the results in the present study of the Cu/ZnO system reveal that the morphology of the Cu particles may change their shape reversibly, depending on the reaction conditions. Thus, the results confirm the wetting/nonwetting behaviour of the Cu/ZnO system. Furthermore, the EXAFS results show that under severe reducing conditions Cu–Zn bulk alloys are present in this system. However, the different methanol synthesis conditions at 220°C, which result in the reversible structural changes, are observed not to be related or associated with significant Cu–Zn alloy formation. By comparing the EXAFS results with FTIR investigations, it is likely that to some extent surface alloying occurs under the more reducing conditions, e.g., when the catalyst is heated to 300°C. In view of this, a combined model (depicted in Fig. 9) is proposed by taking into account both the wetting/nonwetting behaviour and surface alloying. The results of the combined EXAFS/XRD/catalytic study indicate that the wetting/nonwetting of the Cu particles and therefore the change in surface area influences the activity of the catalysts, but alloying at the interface might help the wetting of the support. At higher temperatures, first surface

alloying occurs and finally bulk alloying is observed, which could have an additional effect on the activity as proposed by several authours (14, 19, 23). Alloying and structural transformations were not observed on Cu/SiO_2 catalysts, which shows that such effects are unique for systems containing easily reducible metal oxide supports, e.g., ZnO.

ACKNOWLEDGMENTS

The authors would like to thank H. T. Teunissen and B. S. Hammershøi for preparation of the catalyst samples and C. V. Ovesen, E. Törnqvist, and I. Chorkendorff for helpful discussions and comments. HASYLAB (Hamburg, Germany) is gratefully acknowledged for offering beam time for the combined (Q)EXAFS/XRD experiments at RÖMO II and the Danish Natural Science Research Council for financial support through DANSYNC.

REFERENCES

1. Klier, K., *Adv. Catal.* **31**, 243 (1982).
2. Fleisch, T. H., and Mieville, R. L., *J. Catal.* **90**, 165 (1984).
3. Clausen, B. S., Lengeler, B., and Rasmussen, B. S., *J. Phys. Chem.* **89**, 2319 (1985).
4. Chinchen, G. C., Denny, P. J., Jennings, J. R., Spencer, M. S., and Waugh, K. C., *Appl. Catal.* **36**, 1 (1988).
5. Clausen, B. S., Lengeler, B., Rasmussen, B. S., Niemann, W., and Topsøe, H., *J. Phys. (Paris) C* **8**, 237 (1986).
6. Waugh, K. C., *Catal. Today* **15**, 51 (1992).
7. Frost, J. C., *Nature* **334**, 577 (1988).
8. Clausen, B. S., and Topsøe, H., *Catal. Today* **9**, 189 (1991).
9. Muhler, M., Nielsen, L. P., Törnqvist, E., Clausen, B. S., and Topsøe, H., *Catal. Lett.* **14**, 241 (1992).
10. Ponec, V., *Surf. Sci.* **272**, 111 (1992).
11. Ovesen, C. V., Clausen, B. S., Schiøtz, J., P. Stoltze, Topsøe, H., and Nørskov, J. K., *J. Catal.* **168**, 133 (1997).
12. Topsøe, H., Ovesen, C. V., Clausen, B. S., Yopsøe, N.-Y., Nielsen, P. E. H., Törnqvist, E., and Nørskov, J. K., *in* "Dynamics of Surfaces and Reaction Kinetics in Heterogeneous Catalysis," p. 121. Elsevier Science, Amsterdam, 1997.
13. Topsøe, N.-Y., and Topsøe, H., *Top. Catal.* **8**, 267 (1999).
14. Fujitani, T., and Nakamura, J., *Catal. Lett.* **56**, 119 (1998).
15. Waugh, K. C., *Catal. Lett.* **58**, 163–165 (1999).
16. Rasmussen, P. B., Kazuta, M., and Chorkendorff, I., *Surf. Sci.* **318**, 267 (1994).
17. Rasmussen, P. B., Holmblad, P. M., Askgaard, T., Ovesen, C. V., Stoltze, P., Nørskov, J. K., and Chorkendorff, I., *Catal. Lett.* **26**, 373 (1994).
18. Yoshihara, J., and Campbell, C. T., *J. Catal.* **161**, 776 (1996).
19. Fujitani, T., Nakamura, I., Uchijima, T., and Nakamura, J., *Surf. Sci.* **383**, 285 (1997).
20. Topsøe, N.-Y., and Topsøe, H., *J. Mol. Catal.* **141**, 95 (1999).
21. Spencer, M. S., *Catal. Lett.* **60**, 45 (1999).
22. Viitanen, M. M., Jansen, W. P. A., van Welzenis, R. G., Brongersma, H. H., Brands, D. S., Poels, E. K., and Bliek, A., *J. Phys. Chem. B* **103**, 6025 (1999).
23. Poels, E. K., and Brands, D. S., *Appl. Catal. A* **191**, 83 (2000).
24. Clausen, B. S., Schiøtz, J., Gråbek, L., Ovesen, C. V., Jacobsen, K. W., Nørskov, J. K., and Topsøe, H., *Top. Catal.* **1**, 367 (1994).
25. Askgaard, T. S., Nørskov, J. K., Ovesen, C. V., and Stoltze, P., *J. Catal.* **156**, 229 (1995).
26. Brands, D. S., Poels, E. K., Krieger, T. A., Makarova, O. V., Weber, C., Veer, S., and Bliek, A., *Catal. Lett.* **36**, 175 (1996).
27. Yurieva, T. M., Plyasova, L. M., Makarova, O. V., and Krieger, T. A., *J. Mol. Catal. A: Chem.* **113**, 455 (1996).
28. Nakamura, I., Fujitani, T., Uchijima, T., and Nakamura, J., *J. Vac. Sci. Technol. A* **14**, 1464 (1996).
29. Clausen, B. S., Steffensen, G., Fabius, B., Villadsen, J., Feidenhans'l, R., and Topsøe, H., *J. Catal.* **132**, 524 (1991).
30. Clausen, B. S., Gråbæk, L., Steffensen, G., Hansen, P. L., and Topsøe, H., *Catal. Lett.* **20**, 23 (1993).
31. Sankar, G., and Thomas, J. M., *Top. Catal.* **8**, 1 (1999).
32. Prins, R., and Koningsberger, D. C., *in* "X-ray Absorption: Principles, Applications, Techniques of EXAFS, SEXAFS and XANES" (D. C. Koningsberger and R. Prins, Eds.), p. 321. Wiley, New York, 1988.
33. Bart, J. C. J., and Vlaic, G., *Adv. Catal.* **35**, 1 (1987).
34. Clausen, B. S., Topsøe, H., and Frahm, R., *Adv. Catal.* **42**, 315–344 (1998).
35. Clausen, B. S., *Catal. Today* **39**, 293 (1998).
36. Frahm, R., *Rev. Sci. Instr.* **60**, 2515 (1989).
37. Zabinsky, S. I., Rehr, J. J., Ankiudinov, A., Albers, R. C., and Eller, M. J., *Phys. Rev. B* **52**, 2995 (1995).
38. Lengeler, B., *J. Phys. C* **8**, 75 (1986).
39. Rasmussen, B. S., Nielsen, P. E. H., Villadsen, J., and Hansen, J. B., *Stud. Surf. Sci. Catal.* **31**, 785 (1987).
40. van Dillen, J. A., Geus, J. W., Hermans, L. A. M., and van der Meijden, J., *in* "Proceedings, 6th International Congress on Catalysis, London, 1976" (G. C. Bond, P. E. Wells, and F. C. Tompkins, Eds.), p. 677. The Chemical Society, London, 1977.
41. Scherrer, P., *Gött. Nachr.* **2**, 98 (1918).
42. Clausen, B. S., Gråbaek, L., Topsøe, H., Hansen, L. B., Stolze, P., Nørskov, J. K., and Hansen, O. H., *J. Catal.* **141**, 368 (1993).
43. Clausen, B. S., and Nørskov, J. K., *Top. Catal.* **10**, 221 (2000).
44. Fubini, B., and Giamello, E., *J. Therm. Anal.* **29**, 655 (1984).
45. Wulff, G., *Z. Kristallogr.* **34**, 449 (1901).
46. Boccuzzi, F., Ghiotti, G., and Chiorino, A., *Surf. Sci.* **183**, L285 (1987).
47. Makarova, O. V., Yurieva, T. M., Kustova, G. N., Ziborov, A. V., Plyasova, L. M., Minyukova, T. P., Davydova, L. P., and Zaikovskii, V. I., *Kinet. Catal.* **34**, 608 (1993).
48. Weast, R. C., Astle, M. J., and Beyer, W. H., "Handbook of Chemistry and Physics," 65th ed. CRC Press, Boca Raton, FL, 1985.
49. Pearson, W. B., "A Handbook of Lattice Spacings and Structures of Metals and Alloys," Vol. 4. Pergamon, London, 1958.
50. Hansen, L. B., Stoltze, P., Nørskov, J. K., Clausen, B. S., and Niemann, W., *Phys. Rev. Lett.* **64**, 3155 (1990).
51. Boccuzzi, F., and Chiorino, A., *J. Phys. Chem.* **100**, 3617 (1996).
52. Nakamura, J., Nakamura, I., Uchijama, T., Kanai, Y., Watanabe, T., and Saito, M., *J. Catal.* **160**, 65 (1996).